Nano Research
2019, 12(7): 1571–1577

ISSN 1998-0124 CN 11-5974/O4
https://doi.org/10.1007/s12274-019-2394-8

Research Article

# Can insulating graphene oxide contribute the enhanced conductivity and durability of silver nanowire coating?

Feng Duan[1,2,§], Weiwei Li[1,§], Guorui Wang[1], Chuanxin Weng[1,2], Hao Jin[1], Hui Zhang[1] (✉), and Zhong Zhang[1] (✉)

[1] *CAS Key Laboratory of Nanosystem and Hierarchical Fabrication, CAS Center for Excellence in Nanoscience, National Center for Nanoscience and Technology, Beijing 100190, China*
[2] *University of Chinese Academy of Sciences, Beijing 100149, China*
[§] *Feng Duan and Weiwei Li contributed equally to this work.*

© Tsinghua University Press and Springer-Verlag GmbH Germany, part of Springer Nature 2019
**Received:** 22 January 2019 / **Revised:** 19 March 2019 / **Accepted:** 28 March 2019

## ABSTRACT

As an essential component of flexible optoelectronic devices, transparent conductive films made of silver nanowire (AgNW) have attracted wide attention due to the extraordinary optical, electrical and mechanical properties. However, the application of AgNW coating still faces some challenges to be overcome including large contact resistance and poor durability. Here, we induce insulating graphene oxide over silver nanowire network through solution process to modify the electrical property and provide a protective layer. Strong interaction with substrates reducing the contact resistance of AgNW junctions and extra conductive channels of graphene oxide sheets contributes to the dramatic enhancement in electric property as well as durability. The resulting coating exhibits superior and uniform optoelectronic performances (sheet resistance of ~ 38 Ω·sq$^{-1}$ with 91% transmittance at 550 nm), outstanding stability in harsh environments, strong adhesion, and excellent mechanical flexibility after 3,000 bending cycles at a bending radius of 2.0 mm, which imply the promising application prospects in flexible optoelectronics.

## KEYWORDS

silver nanowires, durability, graphene oxide, transparent electrodes, flexible electronics

## 1 Introduction

With the rise of flexible optoelectronic devices, such as flexible touch panels, solar cells, and organic light-emitting diodes (OLED), the key component—flexible transparent conductive film—has attracted extensive attention in recent years [1–4]. Indium tin oxide (ITO) film is a commercial common-used transparent electrode material with excellent electronic performances as well as good stability. However, its further application is severely hindered by the disadvantages including intrinsic brittleness, material scarcity, and high processing temperature [5–7]. As alternatives to ITO, emerging materials have been reported including conducting polymers [8–10], carbon nanotubes (CNTs) [11], graphene [12–15], and metal nanowires [1, 16–18], among which silver nanowire (AgNW) is one of the most promising candidates for its superior conductivity and simultaneously the easy-to-maintain high transmittance. Nevertheless, there remain some challenges in practical applications. Firstly, the high contact resistance between AgNWs always results in poor conductivity of the entire AgNW networks. Besides, its oxidizability as well as the poor adhesion between AgNW networks and substrates, greatly reduces its stability, including both chemical and mechanical aspects. To date, various strategies have been employed to improve the conductivity to some extent, such as laser- or flash-induced plasmonic welding [19, 20], thermal heating [21], and mechanical pressing [22, 23], whereas it remains difficult to achieve stability at the same time. An efficient solution is to offer a protective layer on top of AgNW networks, for instance, by depositing metal oxides [24–26] or embedding in conductive or optical polymers [27–29], but they either require high-temperature treatment or show low efficiency in conductivity improvement.

On the other side, graphene has been proved to be a potential protective layer to enhance electrical conductivity and stability simultaneously due to its hexagonal arrangements of carbon atoms based two-dimensional (2D) atomic structure [30]. The commonly used is the chemical-vapor-deposited (CVD) graphene [31, 32] or the reduced graphene oxide (rGO) [33, 34]. The CVD graphene is especially vulnerable during the transferring process and inconvenient in scalable production, while the rGO is unsuitable because of the complex reduction process and low transparency [35]. Graphene oxide (GO) is a solution processable insulating material with abundant oxygen-containing groups and high Young's modulus, resulting in strong interaction with other materials and high transparency [36–38]. With these advantages, it brings excellent prospect of improving performance of AgNW networks and several results have been reported [39, 40]. Moon, I. K. et al. has reported GO as a protective layer for AgNW films, yet they focused on the high quality of AgNW films originated from the hydrophilic of graphene oxide sheets [39]. Liang, J. et al. attached the importance of strectchability of the AgNW networks with a soldered GO film [40]. Both of them pay little attention to how GO property affects the quality of AgNW films. Thus, there are still issues in how GO improving the performance of AgNW coating.

In this work, we utilize simple and inexpensive GO as a protective layer for AgNW networks to prepare highly conductive and transparent GO/AgNW hybrid coating. Through all solution process, the covering of ultra-thin GO sheets on top of AgNW coating surprisingly

Address correspondence to Zhong Zhang, zhong.zhang@nanoctr.cn; Hui Zhang, zhangh@nanoctr.cn

contributes to a dramatic decrease of sheet resistance while maintaining high transmittance despite of its insulating nature. Meanwhile, its durability including resistance to the solvent corrosion, high temperature and humidity as well as its interfacial adhesion and mechanical flexibility is greatly improved simultaneously. This simple strategy provides an easy way to produce high performance and stable transparent films to replace existing technologies at low cost in a large scale.

## 2 Experimental

### 2.1 Synthesis of AgNWs

Generally, thinner AgNWs with a higher aspect ratio are beneficial to the opto-electronic property, thus the morphological synthesis of AgNW is of crucial importance [41, 42]. A modified polyol procedure was utilized to synthesize AgNWs with an average diameter of 33 nm and length of 18 μm [43]. In a typical process, a three-necked flask with 50 mL ethylene glycol (EG) solution (Beijing J&K Chemical Company), containing 0.3 g polyvinyl pyrrolidone (PVP) (BOAI NKY PHARMACEUTICALS LTD.) and 5 mg seed hexadecyl trimethyl ammonium bromide (CTAB) (Jinke Fine Chemical Research Institute) was heated to 160 °C using an oil bath pan at gentle stirring speed. After refluxing for 30 min, 10 mL EG solution containing 0.2 g $AgNO_3$ (Beijing J&K Chemical Company) was added at a speed of 3 mL·min$^{-1}$. The mixture was heated at 160 °C for another 30 min to complete the reaction. To remove the excess PVP and nanoparticles, after the mixture cold to room temperature, about 2 times by volume acetone was quickly added to the obtained mixtures containing AgNWs under vigorous stirring. After 1 min vigorous stirring and 5 min standing, the mixtures were layered. The supernatant was pipetted using a plastic burette and the precipitation was re-dispersed in some water or ethanol. This adding-pipetting process was repeated for 3–4 times until the supernatant became transparent. The whole process took about 30 min. Finally, the precipitation was redispersed into isopropanol for further use.

### 2.2 Synthesis of GO sheets

GO was prepared by a modified Hummer's method [44]. GO with different size was obtained by ultrasonication treatment with a power of 400 W of as-prepared GO for 5, 15, and 30 min, respectively. The size of GO is defined as the longer diameter of GO sheets, and calculated through averaged 50 pieces in several scanning electron microscopy (SEM) images. The further oxidized GO was synthesized by adding 50 mg as-prepared GO and 20 mL concentrated nitric acid ($HNO_3$) slowly to 98% concentrated sulfuric acid ($H_2SO_4$), following heated to 90 °C stirring for 24 h. The mixture was diluted to 1,000 mL with deionized water, and purified by vacuum filtration and dialysis process to remove ions in GO suspension, till the suspension was neutral. Finally, the further oxidized GO suspension was treated with ultrasonic with power of 100 W for 10 min and diluted in ethyl alcohol with a concentration of 1.0 mg·mL$^{-1}$ for further use. The rGO was fabricated by reduction of 100 mg as-prepared GO with 10 mL hydroiodic acid (HI) at 95 °C along with stirring for 20 min and at room temperature stirring for 12 h. The mixture was purified by centrifugation at a speed of 1,500 rpm and water washings till the supernatant was limpid, then redispersed in ethyl alcohol for further use.

### 2.3 Fabrication of GO/AgNW hybrid coating

The purified AgNW dispersion was diluted to 0.5 mg·mL$^{-1}$ and spraying coated on polyethylene terephthalate (PET) film or other substrates. Then 1.0 mg·mL$^{-1}$ GO suspension was spin coated on the surface of AgNW coating containing PET or other substrates, and dried in an oven at 100 °C for 5 min.

### 2.4 Fabrication of ITO/AgNW hybrid coating

The purified AgNW dispersion was diluted to 0.5 mg·mL$^{-1}$ and spraying coated on PET film. Then 7.5 wt.% thermosetting ITO nano dispersion (VP Disp LTH2, Evonik Degussa Industries) was spin coated on the surface of AgNW coating containing PET substrate, and cured at 100 °C for 5 min.

### 2.5 Fabrication of touch panel

Two pieces of GO/AgNW/PET films were first cut to a size of 13 cm × 13 cm to form the top and bottom layer with printed silver ink on both layers for signal pin out, respectively. Then insulating dot spacers were printed on the bottom layer, followed with insulating adhesive to attach the top and bottom layer together. Lastly, the pin out circuit was bonded to output signals.

### 2.6 Characterization

SEM studies of AgNWs and GO were characterized with a JEOL JSM-7500F. The transmittance of the flexible conductors was characterized with a UV-Vis spectrophotometer (Shimadzu UV-2501PC). A four-point probe measurement (RTS-9, 4-probe Technology Ltd., China) was used to measure the sheet resistance of the conductors with a probe spacing of 1+/−0.01 mm. An atomic force microscopy (AFM, Dimension 3100) was used to analyse the thickness of the GO coating. A conductive atomic force microscopy (Dimension Icon, Veeco) was used to characterize the morphology with height and current signals.

## 3 Results and discussions

### 3.1 Fabrication of GO/AgNW hybrid coating

The three-step fabrication of GO/AgNW hybrid coating is depicted in Fig. 1(a). The isopropyl alcohol (IPA) dispersed 0.5 mg·mL$^{-1}$ AgNW suspension was firstly spray coated onto a PET or another plastic substrate, which is subsequently covered by ethanolic suspension of GO sheets via spin coating at a rate of 2,000 rpm, finally following with the drying of hybrid coating at 100 °C for 5 min. In order to gain an insight into the optoelectronic property variation of AgNW networks with GO, the sheet resistance and transmittance of as-prepared coatings are measured and summarized in Figs. 1(b) and 1(c), respectively. Here, the "spray times" mean the times that the AgNW suspension is sprayed onto the whole substrate at a moving rate of 4.5 cm·s$^{-1}$ under 0.6 MPa. The increasing spray times indicate a densor AgNW network. Obviously, with the coverage of the GO sheets, a significant reduction in the sheet resistance of GO/AgNW hybrid coating is observed regardless of AgNW density. Specifically, through 60 times of spray coating, the mean sheet resistance of the films with the GO sheets decreases from ~ $10^6$ to 449 Ω·sq$^{-1}$, which is more than three orders of magnitude. Similar phenomena can also be visible when GO/AgNW hybrid coating with different AgNW density is deposited on different substrates, including polycarbonate (PC), poly(methyl methacrylate) (PMMA) and glass (Fig. S1 in the Electronic Supplementary Material (ESM)), which indicates that such method is universal to various substrates for practical application. Meanwhile, the GO/AgNW coating exhibits a negligible decrease but even about 1% improvement in the transmittance within the light wavelength range from 400 to 1,000 nm. This may come from the reduced light scattering for the induce of GO sheets [45]. Moreover, the covering of GO sheets significantly improves the uniformity of sheet resistance distribution for AgNW coating. The large-area transparent conductive GO/AgNW/PET film (13 cm × 13 cm) displays a uniform sheet resistance distribution (averaged 47.2 Ω·sq$^{-1}$) merely with a 12.76% standard deviation, averaged over 169 points within a 1 cm × 1 cm lattice (Fig. 1(d)). In comparison, with the same area, similar AgNW density

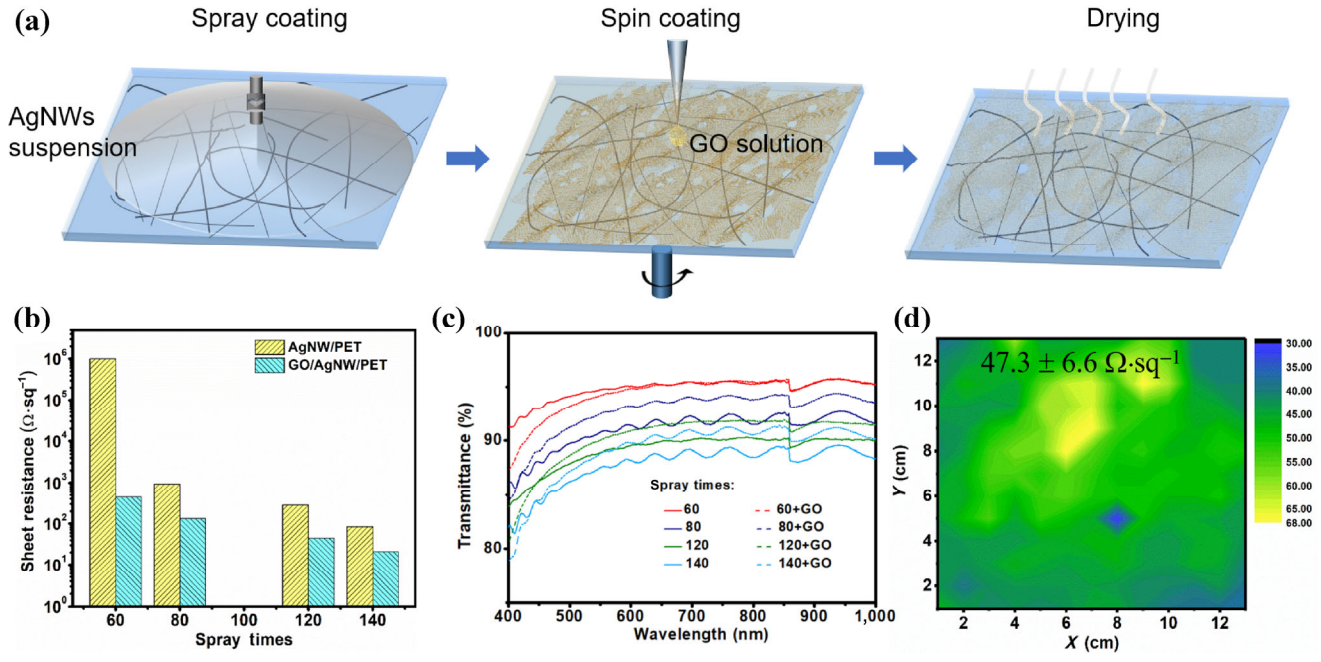


**Figure 1** (a) Schematic illustration of GO/AgNW coating procedure on PET film. (b) and (c) Sheet resistance and transmittance of AgNW coating before and after GO coating. (d) Sheet resistance distribution of GO/AgNW coating on PET film (13 cm × 13 cm).

and transmittance of 91.7% at 550 nm, the ITO/AgNW/PET film shows a sheet resistance as high as 864.3 Ω·sq$^{-1}$, 18 times higher than that of GO/AgNW/PET film, with a 40% standard deviation (Fig. S2 in the ESM). It should be noted that, in striking contrast with graphene, GO typically possesses a broken long-range conjugate structure and hence is insulating with the sheet resistance of ~ $10^{12}$ Ω·sq$^{-1}$ or higher [46, 47]. However, herein, GO sheets counterintuitively play significant roles in enhancing the conductivity of AgNW coating, wherein the underlying mechanisms have yet to be examined and the corresponding key parameters remain elusive.

### 3.2 GO/AgNW hybrid coating with controllable GO sheets

To figure out how GO sheets contribute to the enhanced conductivity of AgNW networks, we examined several parameters including concentration of GO suspension, sheet size, and oxidation degree of GO sheets. Firstly, GO suspension with different concentration was covered on the top of a series of AgNW coating with precisely controlled AgNW suspension concentration and spray times. The sheet resistance of GO/AgNW hybrid coating dramatically decreases by about two orders of magnitude when GO concentration increases from 0.05 to 0.5 mg·mL$^{-1}$, and it decreases gently with a higher concentration of GO (Fig. 2(a)). This attributes to the coverage of GO sheets over AgNW networks changing from independent islands to completely continuous film with the increasing GO concentration, which can be observed from SEM images (Figs. 2(b) and 2(c)). At the same time, the transmittance of hybrid coating shows a slight

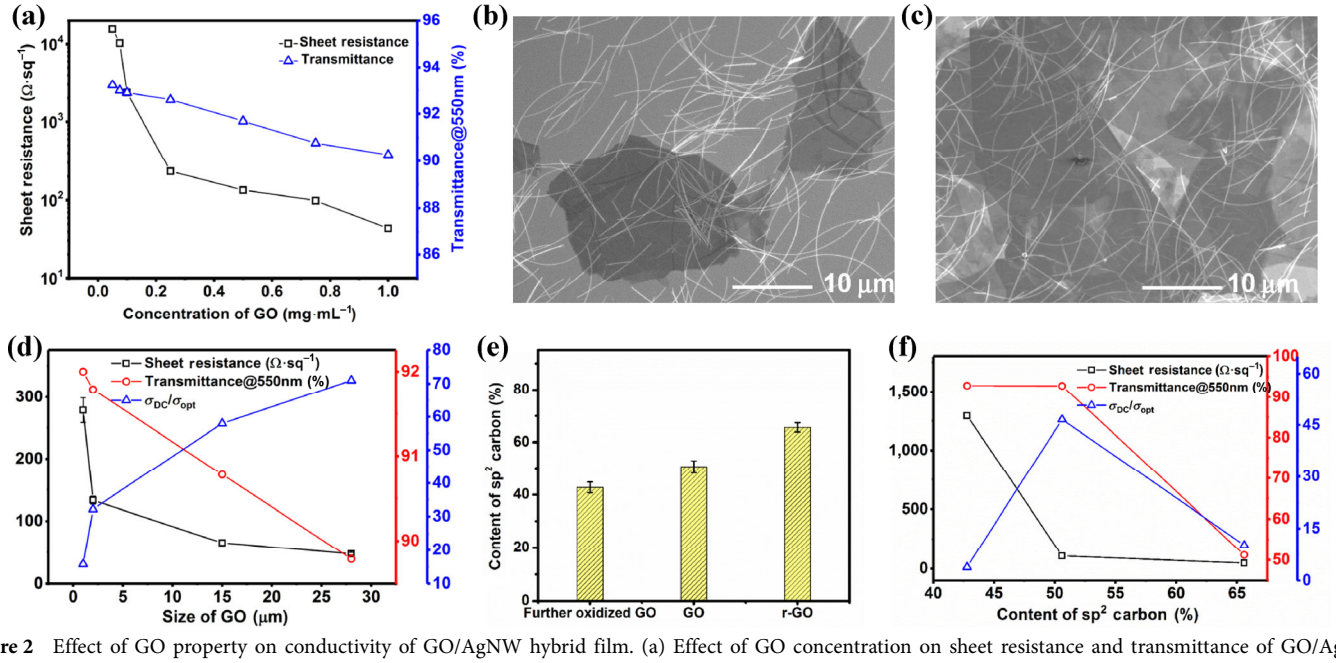


**Figure 2** Effect of GO property on conductivity of GO/AgNW hybrid film. (a) Effect of GO concentration on sheet resistance and transmittance of GO/AgNW coating. (b) and (c) SEM images of GO/AgNW hybrid coating with GO concentration of 0.1 and 1 mg·mL$^{-1}$. (d) Sheet resistance, transmittance and figure of merit of GO/AgNW hybrid coating with different GO size. (e) $sp^2$ carbon content in GO with different oxidation degree. (f) Effect of oxidation degree of GO on sheet resistance, transmittance and figure of merit.

decrease from 93.2% to 90.2% accordingly with increasing thickness of GO films. It's reasonable to find that the conductivity and transmittance of GO/AgNW hybrid coating show an opposite variation trend with the increasing concentration of GO suspension. To further illuminate the influence of GO concentration on the comprehensive property as a transparent film, the figure of merit (FOM) is estimated by using the following equation

$$\frac{\sigma}{\alpha} = \frac{188.5}{R_s(T^{-1/2} - 1)} \quad (1)$$

where $T$ is the optical transmittance measured at a wavelength of 550 nm, which corresponds to the maximum human visual sensitivity, $\sigma$ is electrical conductivity, $\alpha$ is the visible absorption coefficient, and $R_s$ is the sheet resistance [48, 49]. The FOM indicates the ratio of electrical conductivity to the visible absorption coefficient, which is typically used to evaluate the performance of transparent conductive films, where high FOM corresponds to low sheet resistance and high transmittance. The calculated FOM shows a sharp improvement with the increase of GO concentration, as shown in Fig. S3 in the ESM. Especially, FOM increases from 0.34 to 100, improved by two orders of magnitude when GO concentration increases from 0.05 to 1.0 mg·mL$^{-1}$. From the architecture of GO/AgNWs hybrid coating captured by SEM (Fig. 2(c)), we can see that when the GO concentration is 1.0 mg·mL$^{-1}$, GO sheets distribute as a continuous film, completely covering over the AgNW networks. Higher concentration of GO suspension results in increased thickness of GO films and decrease of transmittance, without obvious increase of conductivity.

The size effect of GO sheets on the conductivity and transmittance of hybrid coating is also explored as shown in Fig. 2(d). With the average size increasing from 1 to 28 μm (Figs. S4(a)–S4(d) in the ESM), the decreased tendency can be observed in both sheet resistance (from 278.8 to 47.6 Ω·sq$^{-1}$) and the transmittance at 550 nm wavelength (from 92% to 89.79%) and consequently, the FOM is enhanced from 15.8 to 71.1. From the SEM images (Figs. S4(e) and S4(f) in the ESM) we can figure out that such GO size dependence originates from the different distribution of GO sheets over AgNW networks caused by relative sizes of GO sheets and pores of AgNW networks. For instance, when the average size of pores in AgNW networks is ~ 5 μm, GO sheets with a size of 28 μm can cover completely over the AgNW networks including 10 μm pores, while GO sheets with a size of 1 μm are mostly dispersed on top of substrate or aggregated beside AgNWs. Only those covered or aggregated right on the AgNW junctions can effectively improve the conductivity of AgNW coating, consequently leading to limited improvement of conductivity for AgNW coating.

In addition, to probe the effect of GO structure on the conductivity of hybrid coating, GO with different oxidation degrees was applied to compound with AgNW coating. Different oxidation degrees of GO sheets are obtained by a further oxidation process or reduction process of the as-prepared GO and the oxygen-containing groups identified by X-ray photoelectron spectroscopy (XPS) is shown in Figs. S5(a) and S5(b) in the ESM and Fig. 3(b). The content of sp$^2$ carbon in GO structure is defined as the ratio of sp$^2$ carbon peak area to whole peak area in XPS spectrum. The higher sp$^2$ carbon content indicates a lower oxidation degree, as Fig. 2(e) shows that rGO has the lowest oxidation degree. Given the precisely controlled similar size and concentration of GO covered on top of AgNW networks, the conductivity of hybrid coating presents an increasing trend with growing oxidation degree, as shown in Fig. 2(f). Since rGO has the lowest oxidation degree, percolating pathways among sp$^2$ carbon clusters in rGO films are easily formed to allow carrier transport to occur [44], therefore the hybrid coating covered by rGO shows the highest conductivity. On the other side, for the optical absorption of GO is dominated by π–π* transitions [50], the increasing reduction extent results in the decreased transmittance of rGO films, thus leading to a sharp decrease of transmittance for rGO/AgNW hybrid coating comparing with that of GO/AgNW hybrid coating. It is found that the sp$^2$ carbon in GO structure plays opposite effects on the conductivity and transmittance of hybrid coating. Therefore, there is a balance in oxidation degree of GO to obtain the best performance of AgNWs coating. According to the non-monotone variation trend of the calculated FOM with the increase of GO oxidation degree (Fig. 2(f)), it is suggested that the hybrid coating covered by GO achieves the highest FOM.

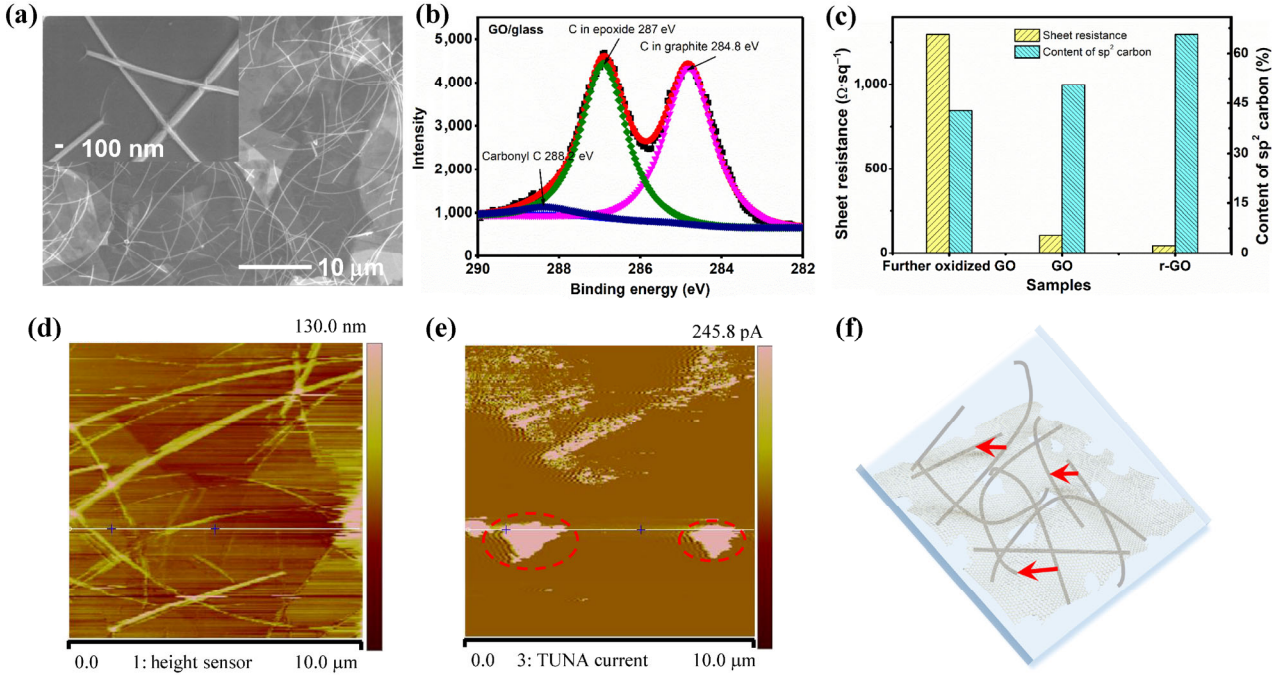


**Figure 3** (a) SEM images of GO/AgNW hybrid coating. (b) C 1s XPS spectrum of GO. (c) Sheet resistance and sp$^2$ carbon content of GO/AgNW hybrid coating with GO of different oxidation degree. (d) and (e) Height image and corresponding current image of GO/AgNW hybrid coating. (f) Schematic possible conductive channels in hybrid coating.

### 3.3 Mechanism discussion

We further investigated the underlying mechanism for improving the conductivity of AgNW coating after covered with GO sheets. From the above analysis, it is reasonable to infer that insulating GO sheets contribute to the conductivity mainly from two aspects: One is that the strong van der Waals force between GO and substrate significantly reduces the junction resistance between AgNWs; the other is that the $sp^2$ carbon clusters existing in GO structure may form percolating pathways combined with AgNWs, resulting in extra conductive channels. The 2D GO sheets have a considerably high diameter-thickness ratio (Fig. S6 in the ESM, average diameter 28 μm, thickness 5 nm with many wrinkles), so that they can cover completely over AgNW networks as shown in the SEM images in Fig. 3(a). The insert of amplified view shows that GO sheets adhere tightly to the surface of AgNWs and substrate. The XPS analysis of carbon 1s spectrum in Fig. 3(b) presents large amounts of oxygen-containing groups including carbon in epoxide at 287 eV and carbonyl carbon at 288 eV in GO structure. The abundant oxygen-containing groups induce strong interaction between GO sheets and substrate, which becomes a driving force for intimate contact among AgNWs and reduces the contact resistance of AgNW junctions significantly, as found in other report [39].

Furthermore, $sp^2$ carbon clusters can connect adjacent AgNWs and form a new conductive path, although the GO sheets are overall insulating with a sheet resistance of ~ $10^{12}$ Ω·sq$^{-1}$ or higher [46, 47] due to the oxygen-containing groups destroying the percolating pathways among $sp^2$ carbon clusters. It can be inferred from Fig. 3(c) that the average sheet resistance of GO/AgNW hybrid coating decreases obviously from 2,070, 310 to 267 Ω·sq$^{-1}$ when the $sp^2$ carbon fraction in GO sheets increases from 42.78%, 50.6% to 65.6%, respectively. Moreover, by comparing conductive AFM images, we observe the conductive $sp^2$ carbon clusters in GO sheets are bridged by AgNWs. The height and current images of GO/AgNW hybrid film in Figs. 3(d) and 3(e) show obvious differences. The morphology of AgNW coating with the covering of GO sheets is conspicuous in height image, while AgNWs cannot be identified clearly in current image owing to the insulating nature of GO sheets. The highlight areas within the red circle in current image exhibit that there exist partial conductive areas in insulating GO sheets. However, in the pure AgNW coating the height and current images show no evident difference but only the morphology of AgNWs (Fig. S7 in the ESM). From the current image of GO/AgNW hybrid coating (Fig. 3(e)), the measured length of the conductive area in insulating GO films in the red circle is ~ 2.2 and 1.4 μm, respectively, which is sufficiently long to connect AgNWs at junctions and form new conductive paths between adjacent AgNWs. The results directly manifest that the $sp^2$ carbon clusters in the GO structure are likely to provide extra conductive paths for hybrid coating, contributing to the improvement of conductivity. Figure 3(f) shows a brief schematic illustration about possible extra conductive channels provided by GO sheet in the hybrid coating, wherein red lines stand for possible conductive paths provided by $sp^2$ carbon in GO sheets.

### 3.4 Durability of GO/AgNW hybrid coating

In order to explore the practicality of GO/AgNW hybrid coating, we tested the chemical and mechanical durability of GO/AgNW hybrid coating on 200 μm-thick PET substrate and made a detailed comparison with that of the pure AgNW coating. Chemical durability was investigated by checking the sheet resistance change after keeping coatings in common solvents or high temperature and humidity atmorsphere for a certain time. The sheet resistance change of AgNW coating with GO sheets is negligible (less than 10%) after soaked in water, acetone, and IPA for 2 h, and much lower after placing in 60 °C, 99% humidity atmosphere for 72 h than that without GO sheets (Fig. 4(a)). The GO/AgNW hybrid coating exhibits excellent corrosion stability, superior to that of the pure AgNW coating. In an extreme environment with 99% humidity at 60 °C, the sheet resistance of AgNW coating increases sharply by more than 5 orders of magnitude after 48 h, and it becomes nonconductive after another 24 h. With the protection of GO sheets, the hybrid coating remains well conductive even after 168 h, exhibiting an outstanding corrosion resistance in high temperature and humidity atmosphere (Fig. 4(b)). The morphologies of the pure AgNW and GO/AgNW hybrid coating were checked after exposure in 99% humidity at 60 °C for 96 h. The AgNWs in the pure AgNW coating are broken down into nanoparticles (Fig. S8(a) in the ESM) for oxidation accelerated with water vapor and high temperature, thus leading to a breakup of conductive paths. On the contrary, AgNWs in GO/AgNW hybrid coating barely change after extreme environment exposure (Fig. S8(b) in the ESM). These

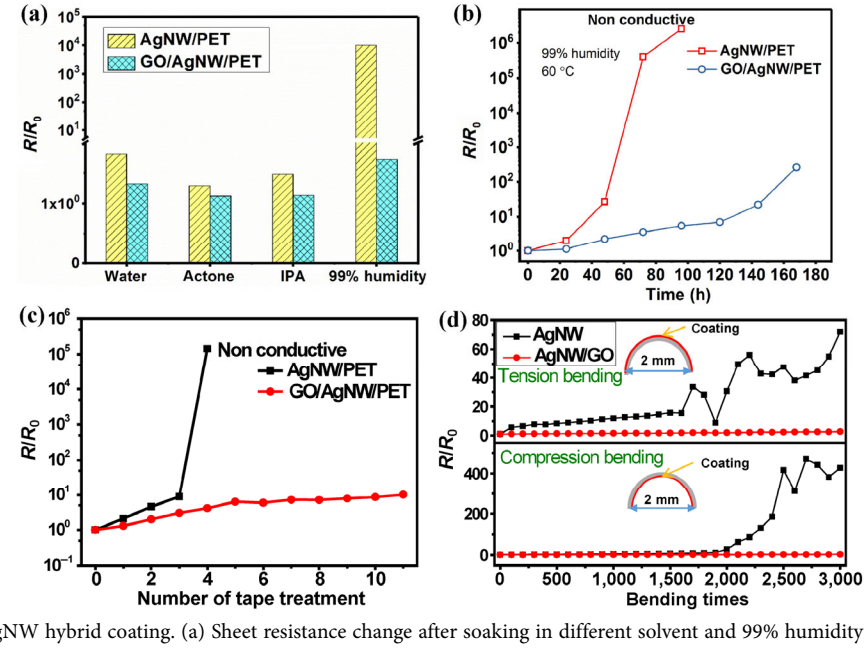


**Figure 4** Durability of GO/AgNW hybrid coating. (a) Sheet resistance change after soaking in different solvent and 99% humidity in room temperature for 2 h. (b) Sheet resistance change after exposure in 99% humidity at 60 °C for different time. (c) Sheet resistance change after 3M tape stick test. (d) Sheet resistance change after different bending cycles under tension and copression bending modes, respectively.

results suggest that the 2D continuous GO film adhereing tightly on substrate endows it with excellent ability to separate AgNWs from contacting with solvents and air and prevent them from oxidation.

To verify the mechanical durability of the hybrid coating, we examined the mechanical adhesion and flexibility of hybrid coating by 3 M Scotch tape detachment test and bending test. The sheet resistance of AgNW coating without GO sheets increases quickly within three times of tape detachment, and it becomes nonconductive after four times of tape detachment, while for the hybrid coating the sheet resistance changes slightly (less than ten times) and remains well conductive after even eleven times of tape detachment as shown in Fig. 4(c). The enhanced adhesion of GO/AgNW hybrid coating also indicates that a strong interaction between GO sheets and substrate guarantees low contact resistance between AgNWs. The flexibility of GO/AgNW hybrid coating was checked by folding the film with a bending radius of 2 mm in both tension and compression modes as shown in Fig. 4(d) and Fig. S9 in the ESM. Subtle change (less than three times) of the sheet resistance for GO/AgNW hybrid coating occurs even after 3,000 cycles of bending in both modes, demonstrating excellent mechanical robust stability and bendability. In contrast, the pure AgNW coating exhibits a dramatic increase of sheet resistance after 2,000 bending cycles in both bending modes, and in tension bending the increase of sheet resistance exceeds 400 times of initial values. The effectively promoted flexibility of GO/AgNW hybrid coating attributes to the tightly covering of GO sheets thus decreasing the dislocation of AgNWs and breakup of conductive path during the bending process.

To demonstrate the practical application of GO/AgNW hybrid coating, a resistive touch panel was fabricated by combining two slices of GO/AgNW/PET films with side of 13 cm × 13 cm separated by insulating dots and integrated with electrodes and the structure is shown in Fig. S10 in the ESM. The superposed two picecs of GO/AgNW/PET films fabricated touch panel exhibits high transparency, as shown in Fig. 5(a) that the word is clearly identified through touch panel. Besides, the touch panel shows good flexibility (Fig. 5(b)). After connecting with computor, the acronym "NCNST" written on touch panel is presented precisely in the display (Fig. 5(c)), implying the possibility of future application in flexible electronics.

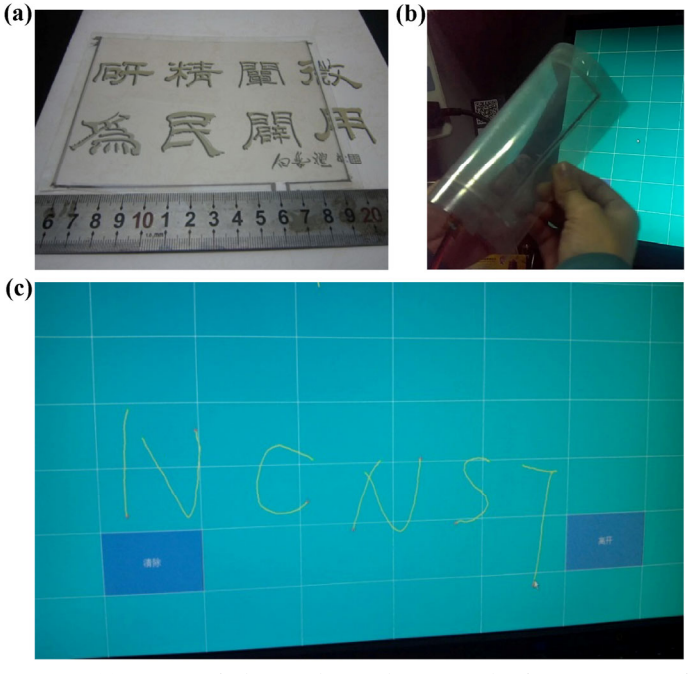


**Figure 5** (a) Image of the touch panel composed of two piceces of GO/AgNW/PET films. (b) Bendability of the as-prepared touch panel. (c) The acronym "NCNST" written by as-prepared touch panel.

## 4 Conclusions

In summary, by combining with insulating GO sheets, we have successfully enhanced the conductivity and uniformity of AgNW coating significantly at the same time with nearly no sacrifice of transparency. Our results show that large GO sheets with low oxidation degree contribute to conductivity by greatly reducing the contact resistance and providing extra conductive channels. Meanwhile, with GO as a separating and protective layer, GO/AgNW hybrid coating exhibits excellent corrosion resistance, strong adhesion, and outstanding mechanical flexibility. The low-cost solution producing process is available for most flexible substrates on a large scale. The obtained solution-processable, conductive, stable, and mechanical robust GO/AgNW coating is expected to have promising applications in flexible electronics.

## Acknowledgements

The work is financially supported by the National Natural Science Foundation of China (Nos. 11890682, 11832010 and 51861165103).

**Electronic Supplementary Material**: Supplementary material (electrical properties of hybrid coating on different substrates; more materials characterization; digtal images of bending test and structure of resistive touch panel) is available in the online version of this article at https://doi.org/10.1007/s12274-019-2394-8.

## References

[1] Chu, H. C.; Chang, Y. C.; Lin, Y.; Chang, S. H.; Chang, W. C.; Li, G. A.; Tuan, H. Y. Spray-deposited large-area copper nanowire transparent conductive electrodes and their uses for touch screen applications. *ACS Appl. Mater. Interfaces* **2016**, *8*, 13009–13017.

[2] Lee, J. W.; Lee, P.; Lee, H. B.; Hong, S.; Lee, I.; Yeo, J.; Lee, S. S.; Kim, T. S.; Lee, D.; Ko, S. H. Room-temperature nanosoldering of a very long metal nanowire network by conducting-polymer-assisted joining for a flexible touch-panel application. *Adv. Funct. Mater.* **2013**, *23*, 4171–4176.

[3] Liu, Z. K.; Li, J. H.; Yan, F. Package-free flexible organic solar cells with graphene top electrodes. *Adv. Mater.* **2013**, *25*, 4296–4301.

[4] Ok, K. H.; Kim, J.; Park, S. R.; Kim, Y.; Lee, C. J.; Hong, S. J.; Kwak, M. G.; Kim, N.; Han, C. J.; Kim, J. W. Ultra-thin and smooth transparent electrode for flexible and leakage-free organic light-emitting diodes. *Sci. Rep.* **2015**, *5*, 9464

[5] Tahar, R. B. H.; Ban, T.; Ohya, Y.; Takahashi, Y. Tin doped indium oxide thin films: Electrical properties. *J. Appl. Phys.* **1998**, *83*, 2631–2645.

[6] Ederth, J.; Johnsson, P.; Niklasson, G. A.; Hoel, A.; Hultåker, A.; Heszler, P.; Granqvist, C. G.; van Doorn, A. R.; Jongerius, M. J.; Burgard, D. Electrical and optical properties of thin films consisting of tin-doped indium oxide nanoparticles. *Phys. Rev. B* **2003**, *68*, 155410.

[7] Kumar, A.; Zhou, C. W. The race to replace tin-doped indium oxide: Which material will win? *ACS Nano* **2010**, *4*, 11–14.

[8] Vosgueritchian, M.; Lipomi, D. J.; Bao, Z. N. Highly conductive and transparent PEDOT:PSS films with a fluorosurfactant for stretchable and flexible transparent electrodes. *Adv. Funct. Mater.* **2012**, *22*, 421–428.

[9] Kim, S.; Sanyoto, B.; Park, W. T.; Kim, S.; Mandal, S.; Lim, J. C.; Noh, Y. Y.; Kim, J. H. Purification of PEDOT:PSS by ultrafiltration for highly conductive transparent electrode of all-printed organic devices. *Adv. Mater.* **2016**, *28*, 10149–10154.

[10] Sun, K.; Li, P. C.; Xia, Y. J.; Chang, J. J.; Ouyang, J. Y. Transparent conductive oxide-free perovskite solar cells with PEDOT:PSS as transparent electrode. *ACS Appl. Mater. Interfaces* **2015**, *7*, 15314–15320.

[11] Jeon, I.; Chiba, T.; Delacou, C.; Guo, Y. L.; Kaskela, A.; Reynaud, O.; Kauppinen, E. I.; Maruyama, S.; Matsuo, Y. Single-walled carbon nanotube film as electrode in indium-free planar heterojunction perovskite solar cells: Investigation of electron-blocking layers and dopants. *Nano Lett.* **2015**, *15*, 6665–6671.

[12] Han, T. H.; Lee, Y.; Choi, M. R.; Woo, S. H.; Bae, S. H.; Hong, B. H.; Ahn, J. H.; Lee, T. W. Extremely efficient flexible organic light-emitting diodes with modified graphene anode. *Nat. Photonics* **2012**, *6*, 105–110.

[13] Liu, Z. K.; You, P.; Xie, C.; Tang, G. Q.; Yan, F. Ultrathin and flexible perovskite solar cells with graphene transparent electrodes. *Nano Energy* **2016**, *28*, 151–157.
[14] Sung, H.; Ahn, N.; Jang, M. S.; Lee, J. K.; Yoon, H.; Park, N. G.; Choi, M. Transparent conductive oxide-free graphene-based perovskite solar cells with over 17% efficiency. *Adv. Energy Mater.* **2016**, *6*, 1501873.
[15] Petridis, C.; Konios, D.; Stylianakis, M. M.; Kakavelakis, G.; Sygletou, M.; Savva, K.; Tzourmpakis, P.; Krassas, M.; Vaenas, N.; Stratakis, E. et al. Solution processed reduced graphene oxide electrodes for organic photovoltaics. *Nanoscale Horiz.* **2016**, *1*, 375–382.
[16] Hu, L. B.; Kim, H. S.; Lee, J. Y.; Peumans, P.; Cui, Y. Scalable coating and properties of transparent, flexible, silver nanowire electrodes. *ACS Nano* **2010**, *4*, 2955–2963.
[17] Fang, Y. S.; Wu, Z. C.; Li, J.; Jiang, F. Y.; Zhang, K.; Zhang, Y. L.; Zhou, Y. H.; Zhou, J.; Hu, B. High-performance hazy silver nanowire transparent electrodes through diameter tailoring for semitransparent photovoltaics. *Adv. Funct. Mater.* **2018**, *28*, 1705409.
[18] Teymouri, A.; Pillai, S.; Ouyang, Z.; Hao, X. J.; Liu, F. Y.; Yan, C.; Green, M. A. Low-temperature solution processed random silver nanowire as a promising replacement for indium tin oxide. *ACS Appl. Mater. Interfaces* **2017**, *9*, 34093–34100.
[19] Nian, Q.; Saei, M.; Xu, Y.; Sabyasachi, G.; Deng, B. W; Chen, Y. P.; Cheng, G. J. Crystalline nanojoining silver nanowire percolated networks on flexible substrate. *ACS Nano* **2015**, *9*, 10018–10031.
[20] Park, J. H.; Hwang, G. T.; Kim, S.; Seo, J.; Park, H. J.; Yu, K.; Kim, T. S.; Lee, K. J. Flash-induced self-limited plasmonic welding of silver nanowire network for transparent flexible energy harvester. *Adv. Mater.* **2017**, *29*, 1603473.
[21] Park, J. W.; Shin, D. K.; Ahn, J.; Lee, J. Y. Thermal property of transparent silver nanowire films. *Semicond. Sci. Technol.* **2014**, *29*, 015002.
[22] Chen, T. L.; Ghosh, D. S.; Mkhitaryan, V.; Pruneri, V. Hybrid transparent conductive film on flexible glass formed by hot-pressing graphene on a silver nanowire mesh. *ACS Appl. Mater. Interfaces* **2013**, *5*, 11756–11761.
[23] Seo, J. H.; Hwang, I.; Um, H. D.; Lee, S.; Lee, K.; Park, J.; Shin, H.; Kwon, T. H.; Kang, S. J.; Seo, K. Cold isostatic-pressured silver nanowire electrodes for flexible organic solar cells via room-temperature processes. *Adv. Mater.* **2017**, *29*, 1701479.
[24] Kim, A.; Won, Y.; Woo, K.; Jeong, S.; Moon, J. All-solution-processed indium-free transparent composite electrodes based on Ag nanowire and metal oxide for thin-film solar cells. *Adv. Funct. Mater.* **2014**, *24*, 2462–2471.
[25] Chen, D.; Liang, J.J.; Liu, C.; Saldanha, G.; Zhao, F. C.; Tong, K.; Liu, J.; Pei, Q. B. Thermally stable silver nanowire-polyimide transparent electrode based on atomic layer deposition of zinc oxide on silver nanowires. *Adv. Funct. Mater.* **2015**, *25*, 7512–7520.
[26] Khan, A.; Nguyen, V. H.; Muñoz-Rojas, D.; Aghazadehchors, S.; Jiménez, C.; Nguyen, N. D.; Bellet, D. Stability enhancement of silver nanowire networks with conformal ZnO coatings deposited by atmospheric pressure spatial atomic layer deposition. *ACS Appl. Mater. Interfaces* **2018**, *10*, 19208–19217.
[27] Kim, Y.; Ryu, T. I.; Ok, K. H.; Kwak, M. G.; Park, S.; Park, N. G.; Han, C. J.; Kim, B. S.; Ko, M. J.; Son, H. J. et al. Inverted layer-by-layer fabrication of an ultraflexible and transparent Ag nanowire/conductive polymer composite electrode for use in high-performance organic solar cells. *Adv. Funct. Mater.* **2015**, *25*, 4580–4589.
[28] Jin, Y. X.; Li, L.; Cheng, Y. R.; Kong, L. Q.; Pei, Q. B.; Xiao, F. Cohesively enhanced conductivity and adhesion of flexible silver nanowire networks by biocompatible polymer sol-gel transition. *Adv. Funct. Mater.* **2015**, *25*, 1581–1587.
[29] Xiong, W. W.; Liu, H. L.; Chen, Y. Z.; Zheng, M. L.; Zhao, Y. Y.; Kong, X. B.; Wang, Y.; Zhang, X. Q.; Kong, X. Y.; Wang, P. F. et al. Highly conductive, air-stable silver nanowire@iongel composite films toward flexible transparent electrodes. *Adv. Mater.* **2016**, *28*, 7167–7172.
[30] Katsnelson, M. I. Graphene: Carbon in two dimensions. *Mater. Today* **2007**, *10*, 20–27.
[31] Chen, R. Y.; Das, S. R.; Jeong, C.; Khan, M. R.; Janes, D. B.; Alam, M. A. Co-percolating graphene-wrapped silver nanowire network for high performance, highly stable, transparent conducting electrodes. *Adv. Funct. Mater.* **2013**, *23*, 5150–5158.
[32] Choi, H. O.; Kim, D. W.; Kim, S. J.; Cho, K. M.; Jung, H. T. Combining the silver nanowire bridging effect with chemical doping for highly improved conductivity of CVD-grown graphene films. *J. Mater. Chem. C* **2014**, *2*, 5902–5909.
[33] Hwang, B.; Park, M.; Kim, T.; Han, S. M. Effect of RGO deposition on chemical and mechanical reliability of Ag nanowire flexible transparent electrode. *RSC Adv.* **2016**, *6*, 67389–67395.
[34] Zhang, X. Q.; Wu, J.; Liu, H.; Wang, J. T.; Zhao, X. F.; Xie, Z. Y. Efficient flexible polymer solar cells based on solution-processed reduced graphene oxide-assisted silver nanowire transparent electrode. *Org. Electron.* **2017**, *50*, 255–263.
[35] Eda, G.; Fanchini, G.; Chhowalla, M. Large-area ultrathin films of reduced graphene oxide as a transparent and flexible electronic material. *Nat. Nanotechnol.* **2008**, *3*, 270–274.
[36] Pei, S. F.; Cheng, H. M. The reduction of graphene oxide. *Carbon* **2012**, *50*, 3210–3228.
[37] Suk, J. W.; Piner, R. D.; An, J.; Ruoff, R. S. Mechanical properties of monolayer graphene oxide. *ACS Nano* **2010**, *4*, 6557–6564.
[38] Zhu, Y. W.; Murali, S.; Cai, W. W.; Li, X. S.; Suk, J. W.; Potts, J. R.; Ruoff, R. S. Correction: Graphene and graphene oxide: Synthesis, properties, and applications. *Adv. Mater.* ***2010,*** *22*, 5226.
[39] Moon, I. K.; Kim, J. I.; Lee, H.; Hur, K.; Kim, W. C.; Lee, H. 2D graphene oxide nanosheets as an adhesive over-coating layer for flexible transparent conductive electrodes. *Sci. Rep.* **2013**, *3*, 1112.
[40] Liang, J. J.; Li, L.; Tong, K.; Ren, Z.; Hu, W.; Niu, X. F.; Chen, Y. S.; Pei, Q. B. Silver nanowire percolation network soldered with graphene oxide at room temperature and its application for fully stretchable polymer light-emitting diodes. *ACS Nano* **2014**, *8*, 1590–1600.
[41] Sun, Y. G.; Gates, B.; Mayers, B.; Xia, Y. N. Crystalline silver nanowires by soft solution processing. *Nano Lett.* **2002**, *2*, 165–168.
[42] Sun, Y. G. Silver nanowires—Unique templates for functional nanostructures. *Nanoscale* **2010**, *2*, 1626–1642.
[43] Sun, Y. G.; Mayers, B.; Herricks, T.; Xia, Y. N. Polyol synthesis of uniform silver nanowires: A plausible growth mechanism and the supporting evidence. *Nano Lett.* **2003**, *3*, 955–960.
[44] Gao, Y.; Liu, L. Q.; Zu, S. Z.; Peng, K.; Zhou, D.; Han, B. H.; Zhang, Z. The effect of interlayer adhesion on the mechanical behaviors of macroscopic graphene oxide papers. *ACS Nano* **2011**, *5*, 2134–2141.
[45] Krantz, J.; Stubhan, T.; Richter, M.; Spallek, S.; Litzov, I.; Matt, G. J.; Spiecker, E.; Brabec, C. J. Spray-coated silver nanowires as top electrode layer in semitransparent P3HT:PCBM-based organic solar cell devices. *Adv. Funct. Mater.* **2013**, *23*, 1711–1717.
[46] Mattevi, C.; Eda, G.; Agnoli, S.; Miller, S.; Mkhoyan, K. A.; Celik, O.; Mastrogiovanni, D.; Granozzi, G.; Garfunkel, E.; Chhowalla, M. Evolution of electrical, chemical, and structural properties of transparent and conducting chemically derived graphene thin films. *Adv. Funct. Mater.* **2009**, *19*, 2577–2583.
[47] Eda, G.; Chhowalla, M. Chemically derived graphene oxide: Towards large-area thin-film electronics and optoelectronics. *Adv. Mater.* **2010**, *22*, 2392–2415.
[48] Ellmer, K. Past achievements and future challenges in the development of optically transparent electrodes. *Nat. Photonics* **2012**, *6*, 809–817.
[49] Lee, H.; Kim, M.; Kim, I.; Lee, H. Flexible and stretchable optoelectronic devices using silver nanowires and graphene. *Adv. Mater.* **2016**, *28*, 4541–4548.
[50] Robertson, J. Diamond-like amorphous carbon. *Mater. Sci. Eng.: R: Rep.* **2002**, *37*, 129–281.